Ambient noise surface wave tomography of the Iberian Peninsula: Implications for shallow seismic structure

Antonio Villaseñor [1], Yingjie Yang [2], Michael H. Ritzwoller [2], and Josep Gallart [1]

[1] Institute of Earth Sciences "Jaume Almera" – CSIC, Lluís Solé i Sabarís s/n, 08028 Barcelona, Spain. E-mail: antonio@ija.csic.es

[2] Center for Imaging the Earth's Interior, Department of Physics, University of Colorado, Campus Box 390, Boulder, CO 80309, USA

Abstract

We have obtained high resolution group velocity maps of Rayleigh waves at periods from 8 to 25 seconds across the Iberian Peninsula by cross-correlating four months of ambient noise data recorded by 40 permanent broadband stations. Group velocity maps accurately image the main structural elements of the Iberian upper crust, including the Iberian Massif, Alpine orogens and major sedimentary basins. The Pyrenees and the Iberian Chain are imaged as relatively high group velocities, in contrast with the Betic Cordillera, which is characterized by low velocities. We explain these low velocities in the Betics by the presence of widespread intramontane basins created in an extensional episode simultaneous with north-south convergence between the African and Eurasian plates. The most prominent low velocity anomaly in the Iberian Peninsula is related to the Guadalquivir Basin, the flysch units of the Campo de Gibraltar, and the sediments of the Gulf of Cadiz.

Introduction

Surface wave tomography using ambient noise is a rapidly expanding imaging technique. The reason for its growing popularity is that it provides significant advantages compared to conventional earthquake tomography. As shown by Shapiro *et al.* [2005], tomography using ambient noise produces surface wave dispersion maps with unprecedented horizontal resolution (100 km or less, depending on the interstation spacing) well correlated with upper crustal features. It can be applied to regions with sparse, inhomogeneously distributed, or even non-existent seismicity, and produces reliable measurements at periods below 10 seconds that are particularly difficult using earthquakes or explosions due to scattering and attenuation. Another advantage of ambient noise tomography over traditional earthquake tomography is the ability to estimate uncertainties based on the repeatability of the measurements.

In this work we explore the feasibility of applying ambient noise tomography to the Iberian Peninsula using some of the recently deployed and upgraded broadband networks in the region. The Iberian Peninsula is in a favorable geographic location because it is surrounded by the water bodies of the Atlantic Ocean in the west and the Mediterranean Sea in the east, which should provide high ambient noise levels with good azimuthal distribution.

The Iberian Peninsula has been the target of a number of surface-wave investigations to determine its crustal and upper mantle structure. Early studies used analog recordings of long period instruments to obtain two-station Rayleigh-wave dispersion measurements [Payo, 1965; Badal *et al.,* 1992]. The deployment during 1988-1989 of the Network of Autonomously Recording Seismographs (NARS, Dost *et al.,* [1984]) as part of the ILIHA project [Paulssen, 1990] provided a significant impulse to surface wave studies in the Iberian Peninsula. Using two-station dispersion measurements, Badal *et al.*

[1996] and Corchete *et al.* [1995] obtained shear-wave images of the lithosphere and asthenosphere beneath the Iberian Peninsula. The shallow structure has also been studied using short period (1-6 seconds) Rg Rayleigh waves from small earthquakes and explosions for different regions of Iberia: northwestern Spain [Sarrate *et al.,* 1993], southeastern Spain [Navarro *et al.* 1997], and more recently the Alboran Sea and Betic Cordillera [Chourak *et al.*, 2001, 2005].

Here we make use for the first time of recently installed broadband stations in the region to investigate the shallow velocity structure of the entire Iberian Peninsula using short period (8-25 seconds) group velocity measurements. This study significantly improves the spatial resolution compared to earlier surface wave studies that used earthquake data and were limited by the small number of available broadband stations and by the sparse and irregular distribution of earthquakes.

Data and method

The main data source for this study has been the recently deployed Spanish National Seismic Network, installed and run by the Instituto Geográfico Nacional (IGN). The IGN operates over 30 broadband stations in the Iberian Peninsula and surrounding regions (Figure 1). We also used stations from the Western Mediterranean Seismic Network (WM), operated by the Real Instituto y Observatorio de la Armada (ROA) and the Universidad Complutense de Madrid (UCM) in cooperation with GEOFON, together with other stations in the region that are part of global networks (Figure 1). Other regional networks also operate broadband stations in the Iberian Peninsula, but have not been included in this study to avoid overweighting certain regions that are already adequately covered.

The methodology used here is very similar to traditional surface-wave tomography using dispersion measurements [e.g. Ritzwoller and Levshin, 1998] except that the

group velocity measurements are not obtained from earthquake waveforms, but from interstation Green's functions generated by cross-correlation of seismic ambient noise. The processing of seismic ambient noise data to obtain dispersion measurements involves several steps that are described in detail by Bensen *et al.* [2007] and are only briefly summarized here.

The first step in data processing involves removing the instrument response, converting the seismogram to velocity, and applying a pre-processing procedure that reduces the effect of earthquakes and compensates for the spectral characteristics of ambient noise. The contamination of ambient noise recordings by earthquakes and non-stationary noise sources near the stations is partly removed by applying the procedure of "temporal normalization" which consists of computing the running average of the absolute value of the waveform amplitude in a window of fixed length and weighting the waveform at the center of the window by the inverse of that average. This is followed by spectral normalization or "whitening", which takes into account that the ambient noise amplitude spectrum is not flat in the frequency band of interest (potentially 1 – 50 seconds or wider). To compensate for this, we divide the full noise spectrum (amplitude and phase) by the smoothed amplitude spectrum, resulting in all frequencies having comparable amplitudes. This broadens the frequency band of the ambient noise signal and reduces the effect of persistent monochromatic sources such as the Gulf of Guinea resonance documented by Shapiro *et al.* [2006].

Second, using these corrected waveforms, we perform cross-correlation between all station pairs. Cross-correlation is performed in the frequency domain using one-day windows. Cross-correlations are then added together (stacked) to obtain longer time series which enhances the signal to noise ratio. Examples of cross-correlations with respect to the same reference station (PAB) are shown in Figure 2 as a record section.

The result of cross-correlation, stacking, and taking the negative time-derivative is a waveform proportional to the Green's function between the two stations (assuming a random isotropic ambient noise wavefield). Third, we measure group velocity dispersion on the Green's functions using the frequency-time analysis (FTAN) methodology [Levshin *et al.,* 1972] exactly in the same way as it is done with earthquake waveforms. Due to the large number of empirical Green's functions that can be generated, however, group velocity measurements are carried out using an automated implementation of FTAN and a careful quality control of the results [Bensen *et al.*, 2007]. Phase velocities are also measured, but their discussion is beyond the scope of this paper. Dispersion measurements with interstation spacing of less than 3 complete wavelengths at each period are discarded. Because of the relatively short time period considered in this study (4 months) it has not been possible to perform a complete analysis of the error estimates using the temporal repeatability of the measurements. However, Bensen *et al.* [2007] find that frequency-dependent signal-to-noise ratio (SNR) is an acceptable proxy for measurement uncertainty, and we use this criterion to select reliable measurements. In particular, we have considered reliable those group velocity measurements that, at the considered period, have values of SNR > 10. Examples of group velocity measurements for selected paths are shown in Figure 3. Finally, we apply a tomographic inversion to the selected group velocity measurements between 6 and 30 s period to obtain fundamental-mode Rayleigh-wave group velocity maps on a 0.5 × 0.5 degree grid across the Iberian Peninsula. The tomography method is that of Barmin *et al.* [2001], which approximately accounts for the spatially extended frequency-dependent sensitivity of the waves by using Gaussian lateral sensitivity kernels. Although the use of spatially extended sensitivity kernels has only a small effect on the estimated maps at the periods considered [Ritzwoller *et al*. 2002], they

help to provide a more accurate estimate of spatial resolution. Resolution is estimated using the method described in Barmin *et al.* [2001], and is equal to the standard deviation of a Gaussian fit to the resolution surface at each location.

Results

From the total number of 780 potential interstation paths we have obtained approximately a 50% of reliable measurements for periods between 10 and 20 s. Among the reasons for not obtaining valid interstation group velocity measurements we find: stations closer than 3 complete wavelengths; poor performance of one or both of the stations during the time period considered; low signal to noise ratio (SNR < 10) of the estimated Green's function. The last two factors would be improved by observing over a longer time period than the 4 months considered here, while the first one is inherent to the network configuration.

Figure 2 shows a record section of Green's functions for interstation paths between station PAB, located near the geometric center of the Iberian Peninsula, and all the other stations (see inset in Figure 2 for location). In the record section it is clearly visible the move-out of the Rayleigh-wave arrivals and the dispersive nature of the empirical Green's functions. It is also worth noting that the causal and acausal signals (arrivals at positive and negative times, respectively) have similar amplitudes, indicating that the sources of ambient noise are well distributed azimuthally. In order to measure group velocities we combine the two-sided signals into a single signal, by averaging the causal and acausal parts.

As mentioned above, the fundamental-mode Rayleigh-wave group velocities are measured using an automatic implementation of FTAN [Bensen *et al.*, 2007]. Figure 3 shows group velocity measurements obtained for some relevant interstation paths (see inset in Figure 2 for locations). Path EPON-PAB, samples exclusively the NW part of

the stable Iberian Massif and is characterized by high velocities, above 3.0 km/s, and small dispersion (approximately flat group velocity curve between 10 and 20 s). In the NE Iberian Peninsula, path EARA-EIBI crosses two sedimentary basins, the Ebro Basin and the Valencia Trough. At short periods (less than 15 s) low group velocities are caused by sediments that reach thicknesses of up to 4 km in the center of the basins. For periods longer than 20 s, however, the dispersion curve is characterized by velocities comparable to those in the Iberian Massif. This occurs because the long period waves are sampling the lower part of the thin, extended transitional crust and uppermost mantle of the Valencia Trough, which has higher velocities than the surrounding regions. The third curve shown in Figure 3 corresponds to the interstation path ESPR-CART that crosses the internal zones of the Betic Cordillera in an E-W direction. Usually for mountain ranges with significant igneous or metamorphic cores one should expect high velocities (e.g. as the Sierra Nevada and Peninsular Ranges in Southern California [Shapiro *et al.*, 2005]). However, for the Betic Cordillera, the dispersion curve is characterized by low group velocities in the entire period range. This anomalous behavior is discussed in the following section.

We inverted these group velocity measurements using the method of Barmin *et al.* [2001] to obtain Rayleigh-wave group velocity maps for the Iberian Peninsula for periods between 6 and 30 seconds. Well constrained maps were determined only for periods between 8 to 25 seconds, due to the number and distribution of reliable measurements as a function of period. We could not obtain reliable maps for very short periods because these require shorter paths (i.e., smaller station spacing) and a sampling rate higher than the 1 sample per second used in this study. On the other hand, long periods would require longer observation times (preferably 2 years) in order to enhance the SNR and longer paths. Figure 4 shows the obtained Rayleigh-wave group velocity

maps for 10 and 20 s period (Figures 4b,d respectively), together with the stations and path distribution used in each case (Figures 4a,c).

To give an estimate of the resolution of the group velocity maps, instead of using the information from the resolution matrix we determined a scalar quantity that represents the spatial resolution. For each grid point of the model we constructed a resolution kernel, which is a row of the resolution matrix, and we fit a 2-D spatial Gaussian function to the kernel and identified the resolution as twice the standard deviation of the Gaussian. In the two group velocity maps shown in Figure 4, we plotted the contour line that corresponds to a spatial resolution of 100. Inside that contour line, features wider than 100 km are well resolved and can be reliably interpreted. This includes most of the interior of the Iberian Peninsula, and corresponds well with the regions with high density of crossing paths in Figures 4a,c.

Discussion

The features observed in the group velocity maps are discussed here qualitatively in terms of the geological and tectonic features of the Iberian crust. Group (and phase) velocity maps at different periods are usually produced as an early step in determining crustal and upper mantle structure, followed by the inversion of these maps for a 3-D shear-wave velocity model. Group velocity maps, therefore, are themselves data, but can be interpreted with care qualitatively given the known sensitivity of surface waves at each period to structures in the crust, particularly shear velocities. In the following discussion, we will consider that the 10 s period map approximately represents an average of shear velocities in the upper 10 km of the crust, while the 20 s map is most sensitive to depths between 15 and 30 km. The maps are also useful for predicting the arrival of surface waves that are used for magnitude estimation and event discrimination. Finally, it should be noted that group velocities sense crustal structures

somewhat differently than phase velocities; their sensitivity kernels are compressed nearer to the surface. This is advantageous for our discussion, given our interest in the shallow crust beneath the Iberian Peninsula.

The largest, most conspicuous feature visible in all the well-resolved group velocity maps (8 - 25 s) is the high velocity region that extends over most of the western Iberian Peninsula (IP). This structure coincides with the surface expression of the Iberian Massif, a Variscan orogen of Hercynian age that forms the core of the IP. The Massif is bounded on its eastern and southern borders by sedimentary basins and Alpine orogens. To the southeast, the border is coincident with the low velocities associated with the Guadalquivir Basin and the external zones of the Betic Cordillera, although in the 10 s map a zone of high velocities between 2° and 4° W extends to the Mediterranean Sea (Figure 4b). To the east, the Iberian Massif is bounded by the Duero and Tagus basins. In the 10 s map, the boundary between high and low velocities lies slightly to the east of the western surface boundary of the basins, coincident with the region where sediment thickness is smaller. At 20 s period, the southern boundary of the Iberian Massif is very clearly defined, and the extent of the high velocities in the center of the IP has been reduced , with the NW-SE boundary of the Iberian Massif noticeably displaced to the south. Similarly the Cantabrian and Astur-Leonese zones in the northern Iberian Massif at 20 s period are imaged as having average to slightly low velocities and most of north-central and eastern Spain is characterized by relative low velocities.

Another noticeable high velocity anomaly in the 10 s map corresponds in location and strike (SE-NW) with the Iberian Chain (or Iberian Ranges). The Iberian Chain is an intraplate fold belt formed by the inversion of a Mesozoic basin. The high velocities are associated with the central part of the range, where the Paleozoic basement is exposed at

the surface, while Mesozoic sediments have lower velocities. The size and amplitude of the high velocity anomaly decreases noticeably in the 20 s map. This behavior is common to other mountain ranges with igneous and/or metamorphic internal zones that at short periods (shallow depths) are characterized by high velocities, while at longer periods exhibit average or low velocities (in presence of deep crustal roots). The Pyrenees also seem to be characterized by high velocities in the 10 s map, but the extent and shape of the anomalies are not well constrained because of the lack of crossing rays, being outside of the well-resolved part of the model. On the other hand, the Betic Cordillera, the other major Alpine chain in the region, is characterized by low velocities at all analyzed periods (see for example path ESPR-CART in Figure 3). We believe that the lack of high group velocities at short periods in the Betics is caused by the presence of widespread intramontane Neogene-Quaternary basins. These basins were formed by the extensional collapse of the orogen, simultaneous with convergence between Africa and Iberia. The mechanism of this collapse is still poorly understood.

The most evident low velocity anomalies in the 10 s map coincide with the major Cenozoic sedimentary basins in and around the IP. The marine Alboran Basin, between southern Spain and northern Africa, is poorly imaged in this study because of the small number of available broadband stations in northern Africa, although in the 10 s map (Figure 4b) the eastern part of the basin is characterized by low velocities, while the western part is mostly unsampled. The other major marine basin inside the region of this study is the Valencia Trough. This basin is better imaged due to the presence of stations in the Balearic Islands (Figure 1), although the ray path crossing is not optimal. Very low group velocities are obtained for the Valencia Trough, in agreement with the sediment thickness distribution, which reaches 2 to 4 km in the western part of the basin, closest to the Iberian coast [Watts and Torné, 1992].

The four major river basins in the Iberian Peninsula (Ebro, Duero, Tagus, and Guadalquivir) are also imaged as low velocity anomalies. The Ebro and Duero basins are imaged as a single, east-west trending anomaly. Sediment thickness in the Ebro basin is greater in its northern part, close to the Pyrenees foreland, reaching 2 to 4 km depth to the north of the current position of the Ebro river. This asymmetric character is also reproduced in the 10 s group velocity map, with the center of the low-velocity anomaly located in the northern part of the basin. The eastern part of the Ebro Basin is not well resolved due to the lack of crossing paths in northeastern Spain (Figure 4a). However, the most pronounced low velocity anomaly is located in southernmost Spain. The anomaly encompasses different units: the Guadalquivir foreland basin, the western termination of the external zones of the Betic Cordillera, and the flysch units of the Campo de Gibraltar. These flysch units consist mostly of unmetamorphosed deep-water turbidite deposits from Early Cretaceous to Early Miocene that were thrust over the western Betics. The predominance of sediments of marine origin in this region causes very low velocities on average, and the appearance of a single basin in spite of being formed of different units. The very low velocity anomalies associated with these units of imbricate thrust belts (the Betics external zones and the Campo de Gibraltar flyschs) most likely continue to the west into the complex and thick sedimentary sequences of the Gulf of Cadiz [Maldonado *et al.*, 1999].

The group velocity map at 20 s period displays similar features to the map at 10 s, with high velocities in the Iberian Massif and significant low velocities in the southernmost IP and along the Betic Cordillera. However, a significant difference is that the marine basins of the Alboran Sea and Valencia Trough are now characterized by high velocities, which indicates that waves at these periods already sample extended lower crust or uppermost mantle.

The westernmost part of the IP is poorly imaged in this study due to the lack of stations in central and southern Portugal. Therefore, we are not able to image important features such as the thick Mesozoic cover of the Lusitanian Basin that reaches in some parts thicknesses of over 4 km.

In summary, we have obtained detailed Rayleigh wave group velocity maps between 8 and 25 s period for the IP that image with unprecedented detail all major structural elements including the stable Iberian Massif, sedimentary basins and mountain ranges. The only similar previous study is that of Payo *et al.,* [1993] who obtained group velocity maps for short-period Rayleigh waves in the IP, using long-period analog recordings of earthquakes. Their maps, although with a much less dense path coverage, also image high velocities in the center of the Iberian Peninsula and low velocities in southernmost Spain and the gulf of Cadiz, but their resolution and correlation with surface geology is much lower. These results are the first to make use for surface-wave tomography of the newly installed broadband stations in the IP, and are a first step for the determination of a 3-D shear-wave velocity model for the region. This would require obtaining group velocity maps for both shorter and longer periods, and with better spatial coverage and resolution. This will be accomplished by considering longer observation times (at least two years) and incorporating existing and future broadband stations in key areas, such as Portugal and northern Morocco.

Acknowledgments

We thank Resurrección Antón and Carmen López from the Instituto Geográfico Nacional for providing the waveform data from the Spanish National Network used in this study. Data for other stations in the region (with network codes IU, WM, GE, and MN) were obtained from the IRIS and GEOFON data centers. Andrés Pérez-Estaún provided very helpful comments on the manuscript. This work was supported by the

“Ramón y Cajal” programme to AV and by the MEC project CGL2006-01171/BTE. This is a contribution of the Team Consolider-Ingenio 2010 CSD2006-00041 (TOPO-IBERIA). US researchers were supported by a contract from the US Department of Energy, contract DE-FC52-2005NA26607.

References

Badal, J., V. Corchete, G. Payo, F.J. Serón, J.A. Canas, and L. Pujades (1992), Deep structure of the Iberian Peninsula determined by Rayleigh wave velocity inversion, *Geophys. J. Int., 108,* 71-88.

Badal, J., V. Corchete, G. Payo, L. Pujades, and J.A. Canas (1996), Imaging of shear-wave velocity structure beneath Iberia, *Geophys. J. Int., 124,* 591-611.

Barmin, M.P., M.H. Ritzwoller, and A.L. Levshin (2001), A fast and reliable method for surface wave tomography, *Pure Appl. Geophys., 158,* 1351-1375.

Bensen, G.D, M.H. Ritzwoller, M.P. Barmin, A.L. Levshin, F. Lin, M.P. Moschetti N.M. Shapiro, and Y. Yang. (2007), Processing seismic ambient noise data to obtain reliable broad-band surface wave dispersion measurements, in press, *Geophys. J. Int.* (http://ciei.colorado.edu/pubs/2007/2.pdf).

Chourak, M., J. Badal, V. Corchete, and F.J. Serón (2001), A survey of the shallow structure beneath the Alboran Sea using Rg-waves and 3D imaging, *Tectonophysics, 335,* 255-273.

Chourak, M., V. Corchete, J. Badal, F. Gomez, and F. J. Serón (2005), Shallow seismic velocity structure of the Betic Cordillera (Southern Spain) from modelling of Rayleigh wave dispersion, *Surveys in Geophysics, 26,* 481–504.

Corchete, V., J. Badal, F.J. Serón, and A. Soria (1995), Tomographic images of the Iberian subcrustal lithosphere and asthenosphere, *J. Geophys. Res.,* 100, 24133-24146.

Dost, B., A. van Wettum, and G. Nolet (1984), The NARS array, *Geol. Mijnbouw, 63,* 318-386.

Levshin, A.L., Pisarenko, V.F., and G.A. Pogrebinsky (1972), On a frequency-time analysis of oscillations, Ann. Geophys., 28, 211-218.

Maldonado, A., L. Somoza, and L. Pallarés (1999), The Betic orogen and the Iberian-African boundary in the Gulf of Cadiz: geological evolution (central North Atlantic), *Mar. Geol., 155,* 9-43.

Navarro, M., V. Corchete, J. Badal, J.A. Canas, L. Pujades, and F. Vidal (1997), Inversion of Rg waveforms recorded in southern Spain, *Bull. Seism. Soc. Am., 87,* 847-865.

Paulssen, H. (1990). The Iberian Peninsula and the ILIHA Project, *Terra nova, 2,* 429-435.

Payo, G. (1965), Iberian Peninsula crustal structure from surface waves dispersion, *Bull. Seism. Soc. Am., 55,* 727-743.

Payo, G., E. de Ancos, and J. Badal (1993), Short period surface waves in the Iberian region. Part I. Group-velocity contour-lines, *Tectonophysics, 221,* 107-110.

Ritzwoller, M.H., and A.L. Levshin (1998), Eurasian surface wave tomography: group velocities, *J. Geophys. Res., 103,* 4839-4878.

Ritzwoller, M.H., N.M. Shapiro, M.P. Barmin, and A.L. Levshin (2002), Global surface wave diffraction tomography, *J. Geophys. Res.,* 107(B12), 2335, doi:10.1029/2002JB001777.

Sarrate, J., J.A. Canas, L. Pujades, J. Badal, V. Corchete, and G. Payo (1993), Shallow structure of part of northwestern Iberia from short-period Rayleigh-wave observations, *Tectonophysics, 221,* 95-105.

Shapiro, N.M., M. Campillo, L. Stehly, and M.H. Ritzwoller (2005), High-resolution surface-wave tomography from ambient seismic noise, *Science, 307,* 1615-1618.

Shapiro, N.M., M.H. Ritzwoller, and G.D. Bensen (2006), Source location of the 26 sec microseism from cross correlations of ambient seismic noise, *Geophys. Res. Lett.*, 33, L18310, doi:10.1029/2006GL027010.

Vergés, J., and M. Fernàndez (2006), Ranges and basins in the Iberian Peninsula: their contribution to the present topography, *Geological Society of London Memoirs*, 32, 223–234.

Watts, A.B., and M. Torné (1992), Crustal structure and the mechanical properties of extended continental lithosphere in the Valencia Trough (western Mediterranean), *J. Geol. Soc. London, 149,* 813-827.

Figure captions

Figure 1. Structural map of the Iberian Peninsula, showing the major sedimentary basins and the location of the seismic stations used in this study (modified from Vergés and Fernàndez, 2006). Different station symbols indicate network affiliation and are explained in the inset. AB: Alboran Basin; ALZ: Astur-Leonese Zone; BI: Balearic Islands; CG: Campo de Gibraltar flysch units; CS: Central System; CZ: Cantabrian Zone; DB: Duero Basin; EB: Ebro Basin; GB: Guadalquivir Basin; IR: Iberian Range; LB: Lusitanian Basin; TB: Tagus Basin.

Figure 2. Record section of raw (unfiltered) cross correlations of stations in the Iberian Peninsula with respect to station PAB obtained using 4 months of ambient noise data. The causal (positive time) and acausal (negative time) arrivals of the Rayleigh wave are clearly visible in all records. The inset shows the location of the paths corresponding to the record section shown in this figure (thin gray lines) and of the group velocity measurements shown in Figure 3 (thick black lines).

Figure 3. Example of group velocity measurements of fundamental-mode Rayleigh waves from ambient noise cross correlations for interstation paths sampling different structural units of the Iberian region (see Figure 2 for location). The station codes for the two stations that define each path are also indicated.

Figure 4. Ray path coverage and group velocity maps obtained for the 10 and 20 s period Rayleigh waves: a) ray path coverage of 10 s group velocity Rayleigh wave measurements used in the tomographic inversion, b) Rayleigh wave group velocity map at 10 s, c) ray path coverage of 20 s group velocity Rayleigh wave measurements used in the tomographic inversion, b) Rayleigh wave group velocity map at 20 s.

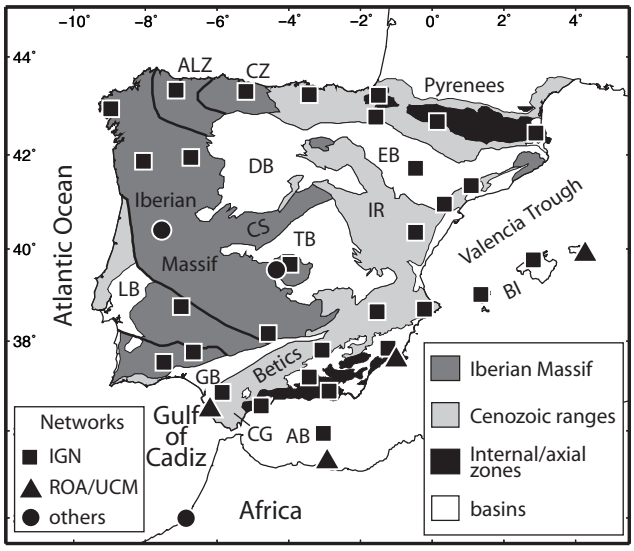
−10°
−8°
−6°
−4°
−2°
0°
2°
4°
44°
42°
40°
38°
ALZ
CZ
Pyrenees
DB
EB
Iberian
Massif
CS
IR
TB
Valencia Trough
BI
LB
Atlantic Ocean
GB
Betics
Gulf
of
Cadiz
CG
AB
Africa
Networks
IGN
ROA/UCM
others
Iberian Massif
Cenozoic ranges
Internal/axial zones
basins

Figure 1

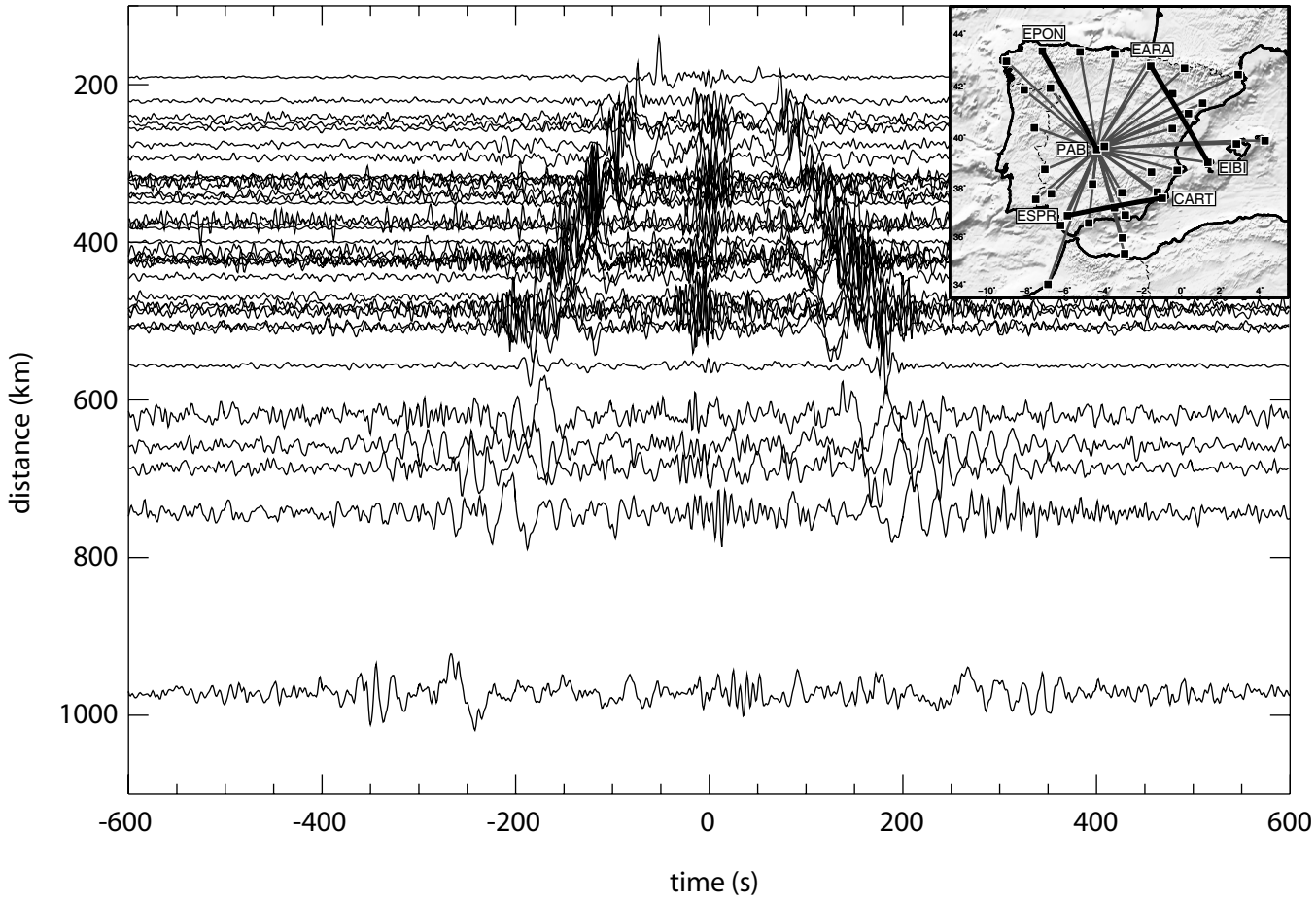
EPON
EARA
PAB
EIBI
CART
ESPR
200
400
600
800
1000
distance (km)
-600
-400
-200
0
200
400
600
time (s)

Figure 2

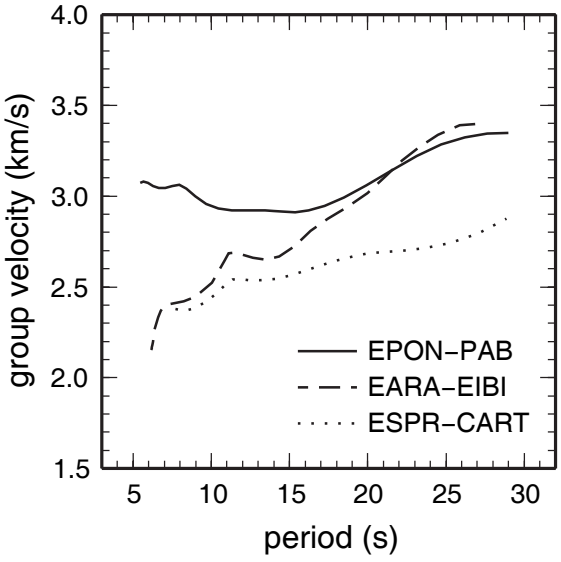
4.0
3.5
3.0
2.5
2.0
1.5
group velocity (km/s)
5
10
15
20
25
30
period (s)
EPON–PAB
EARA–EIBI
ESPR–CART

Figure 3

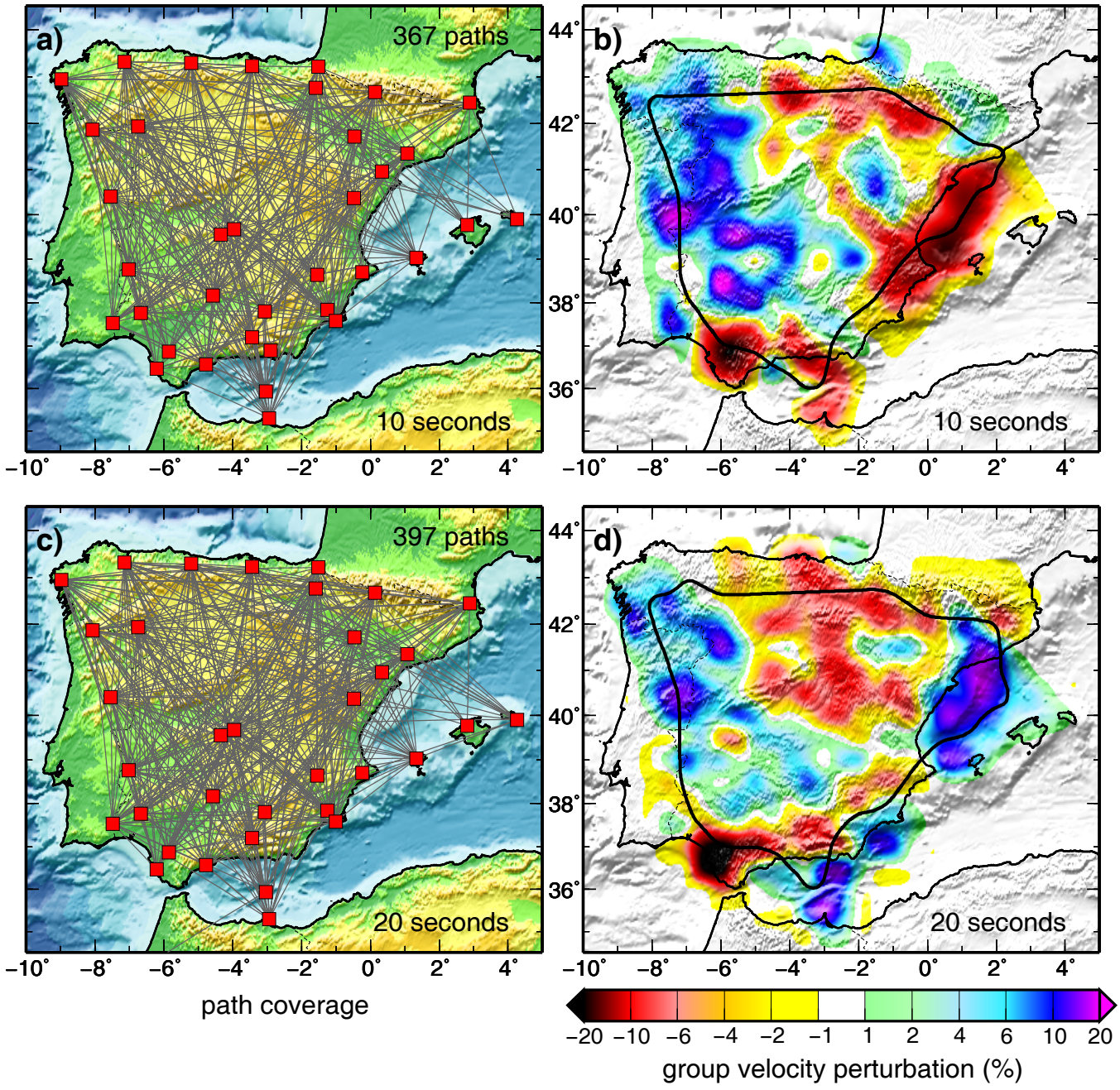
a)
367 paths
10 seconds
b)
10 seconds
c)
397 paths
20 seconds
d)
20 seconds
44°
42°
40°
38°
36°
−10° −8° −6° −4° −2° 0° 2° 4°
path coverage
−20 −10 −6 −4 −2 −1 1 2 4 6 10 20
group velocity perturbation (%)

Figure 4